
E-CAR: Efficient Continuous Autoregressive Image Generation via Multistage Modeling

Zhihang Yuan^{1,2*} Yuzhang Shang^{3*} Hanling Zhang^{1,2} Tongcheng Fang¹ Rui Xie^{1,2}
 Bingxin Xu³ Yan Yan³ Shengen Yan⁴ Guohao Dai^{4,2} Yu Wang¹

¹Tsinghua University ²Infinigence AI ³Illinois Tech ⁴Shanghai Jiao Tong University

Abstract

Recent advances in autoregressive (AR) models with continuous tokens for image generation show promising results by eliminating the need for discrete tokenization. However, these models face efficiency challenges due to their sequential token generation nature and reliance on computationally intensive diffusion-based sampling. We present E-CAR (Efficient Continuous Auto-regressive Image Generation via Multistage Modeling), an approach that addresses these limitations through two intertwined innovations: ❶ a stage-wise continuous token generation strategy that reduces computational complexity and provides progressively refined token maps as hierarchical conditions, and ❷ a multistage flow-based distribution modeling method that transforms only partial-denoised distributions at each stage comparing to complete denoising in normal diffusion models. Holistically, E-CAR operates by generating tokens at increasing resolutions while simultaneously denoising the image at each stage. This design not only reduces token-to-image transformation cost by a factor of the stage number but also enables parallel processing at the token level. Our approach enhances computational efficiency and aligns naturally with image generation principles by operating in continuous token space and following a hierarchical generation process from coarse to fine details. Experimental results demonstrate that E-CAR achieves comparable image quality to DiT [Peebles & Xie, 2023] while requiring $10\times$ FLOPs reduction and $5\times$ speedup to generate a 256×256 image.

1 Introduction

Autoregressive (AR) Large Language Models (LLMs) [Vaswani, 2017, Achiam et al., 2023, Touvron et al., 2023a,b, Jiang et al., 2023] have demonstrated remarkable capabilities in natural language generation, driven by scaling laws [Kaplan et al., 2020, Hoffmann et al., 2022]. Inspired by these advancements, the computer vision community has been striving to develop large autoregressive and world models [Zhou et al., 2024, Team, 2024, Liu et al., 2024a] for visual generation. This effort is initiated by VQ-GAN [Esser et al., 2021] and further advanced by its successors [Lee et al., 2022, Sun et al., 2024, Tian et al., 2024, Team, 2024], showcasing the potential of AR models in visual generation.

Traditional AR image generation models employ a visual tokenizer to discretize continuous images into grids of 2D tokens, which are then flattened into a 1D sequence for AR learning (see Fig. 2.b). However, recent research [Li et al., 2024, Tschannen et al., 2023, Zhou et al., 2024, Fan et al., 2024] demonstrates that discrete tokenization is not only unnecessary but potentially detrimental to AR models’ generation capabilities. These works show that AR image generation can be formulated continuously, modeling per-token probability distributions on continuous-valued domains. For

*Equal Contribution.

instance, several approaches [Li et al., 2024, Zhou et al., 2024, Fan et al., 2024] leverage diffusion models for representing arbitrary probability distributions, where the model autoregressively predicts a continuous vector for each token as conditioning for a denoising network (see Fig. 2.c). We refer to this paradigm as *continuous AR* models.

Despite their advantages, continuous AR models, such as MAR [Li et al., 2024], face significant efficiency challenges. Generating a 256×256 image with MAR using one NVIDIA A5000 GPU requires more than 30 seconds, making these models impractical for real-time applications. We identify two main efficiency bottlenecks: ❶ **Token-by-token generation**: Similar to text generation in LLMs, the sequential token-by-token nature of generation limits efficiency [Yuan et al., 2024]. ❷ **Diffusion-based sampling**: The sampling process inherits the inefficiencies of diffusion models [Song et al., 2020a,b], requiring hundreds of denoising network inferences for token-to-image sampling. Beyond the direct computational costs, these issues significantly constrain parallelization potential, as the token generation process must proceed sequentially.

In this work, we propose Efficient Continuous Autoregressive Image Generation via Multistage Modeling (E-CAR) to address these limitations while maintaining generative capability. As shown in Fig. 1, E-CAR progressively generate tokens at increasing resolutions while simultaneously transport towards the image distribution via a multistage flow at each stage. Our approach features two intervened innovations targeting the efficiency bottleneck: ❶ **Stage-wise Progressive Token Map Generation**: A hierarchical AR transformer architecture that generates continuous tokens at stage-wisely increasing resolutions (*i.e.*, continuous token map), reducing token generation computation by enabling parallel processing within each stage. ❷ **Multistage Flow-based Distribution Modeling**: A flow-based method that transforms continuous token distributions at multiple stages, requiring only partial transport at each resolution level instead of complete denoising processes. This design reduces continuous detokenization computation proportionally to the number of stages. The stage-wise design of our approach enables parallel token sampling, as tokens are generated in resolution-specific stacks. From a flow matching perspective [Ma et al., 2024, Lipman et al., 2022, Liu et al., 2022, Liu, 2022], our multistage approach can be viewed as using the AR model to guide the flow model’s visual generation process, creating a complementary relationship between continuous token generation and flow-based image synthesis.

Importantly, E-CAR’s multistage continuous AR solution aligns naturally with image generation’s pyramidal principles [Pernias et al., 2023, Saharia et al., 2022]. By operating in a continuous token space, it better reflects the inherent structure of images—a widely accepted inductive bias in computer vision [Li et al., 2024]. The increasing resolution generation mirrors the hierarchical nature of visual information, progressing from coarse structures to fine details, enabling effective multi-scale image generation while maintaining high quality [Jin et al., 2024]. To the best of our knowledge, this is the first work that integrates continuous AR and flow-based method in a multistage manner, offering a novel approach to efficient, high-quality visual generation.

2 Related Work

Autoregressive Visual Generation models initially operated on sequences of pixels [Gregor et al., 2014, Van Den Oord et al., 2016, Chen et al., 2018a, 2020]. While early implementations primarily utilized RNNs and CNNs as base models, Transformers [Vaswani, 2017] have recently become the dominant architecture for these tasks [Esser et al., 2021]. VQGAN [Esser et al., 2021] pioneered the use of Transformers for autoregressive image generation. Specifically, it employs a GPT-2 decoder-only Transformer [Radford, 2018] to generate tokens in a raster-scan order, similar to how ViT [Dosovitskiy, 2020] serializes 2D images into 1D patches. Building upon this paradigm, [Razavi et al., 2019, Lee et al., 2022] extend the approach by incorporating multiple scales or stacked codes. More recently, LlamaGen [Sun et al., 2024], based on the popular open-source

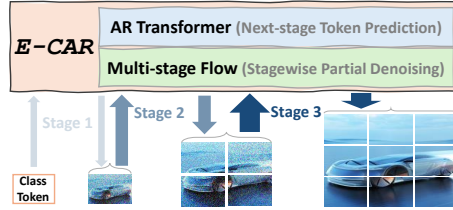


Figure 1: **High-level Idea of E-CAR.** The model progressively generates tokens at increasing resolutions, while correspondingly denoising the image at each stage. By combining stage-by-stage continuous token generation with multistage flow-based image synthesis, E-CAR achieves efficient continuous autoregressive image generation while maintaining high visual quality.

LLM architecture Llama [Touvron et al., 2023a,b], scales the Transformer to 3B parameters and demonstrated impressive results in text-to-image synthesis. In parallel, recent advancements have focused on continuous-valued tokens in AR models. GIVT [Tschannen et al., 2023] represents token distributions using Gaussian mixture models with a pre-defined number of mixtures. MAR [Li et al., 2024] leverages the effectiveness of the diffusion process for modeling arbitrary distributions. We categorize these AR methods that do not use discrete tokenizers as *continuous AR* methods.

Our work focuses on improving the efficiency of continuous AR models. To achieve this, we propose using a multistage AR Transformer to generate continuous tokens stage-by-stage, coupled with a multistage flow-based method to model the token distributions.

Diffusion Models and Flow Matching Models. Diffusion models [Sohl-Dickstein et al., 2015, Ho et al., 2020, Song et al., 2020b] have demonstrated remarkable success across various generative modeling tasks, such as the generation of images, videos, and audio [Croitoru et al., 2023]. Predominantly, these models utilize stochastic differential equations (SDEs) to model the diffusion and denoising processes. [Song et al., 2020b,a] also converted these SDEs into ordinary differential equations (ODEs) that preserve the marginal probability distributions, thereby accelerating the denoising process. Recent research [Liu et al., 2022, Liu, 2022, Lipman et al., 2022] has introduced novel methods for directly learning probability flow ODEs, employing both linear and nonlinear interpolation techniques between distributions. These ODE-based approaches rival the performance of conventional diffusion models while substantially reducing the number of inference steps required. The practical applications of flow matching have expanded beyond theoretical frameworks, with recent investigations applying these methods to larger datasets and more complex tasks. For example, [Liu et al., 2024b] showcased the Rectified Flow pipeline’s capability to produce high-fidelity, one-step generation in large-scale text-to-image (T2I) diffusion models. This advancement has paved the way for extremely rapid T2I foundation models trained exclusively through supervised learning. The influence of these developments is evident in cutting-edge T2I systems, such as Stable Diffusion 3 [Esser et al., 2024], which incorporates reflow as a fundamental component of its generation process.

Our work focuses on continuous AR, but we formulate the distribution estimation under the framework of multistage flow matching, offering a more efficient method for continuous distribution matching.

3 E-CAR: Efficient Continuous Auto-regressive Image Generation via Multistage Modeling

We first review the basic pipeline of continuous autoregressive (AR) visual generation models (Sec.3.1). Next, we introduce our **Efficient Continuous AR** (E-CAR) image generation model. The development and optimization of E-CAR include three key advancements: (1) a stage-by-stage continuous token generation AR module (Sec.3.2); (2) an multistage flow model for fast continuous token recovery (Sec. 3.3); and (3) the multistage loss that enhances training stability (Sec.3.4). Finally, we provide a straightforward explanation of why E-CAR can be both efficient and effective (Sec.4.3).

3.1 Preliminaries: Continuous Autoregressive Visual Generation

The review of continuous AR visual generation models focuses on their main components and training procedures. In this review, we highlight the inefficiencies associated with existing continuous AR models.

Image Tokenization and Detokenization. Images are inherently 2D continuous signals. Pioneering AR studies [Esser et al., 2021, Sun et al., 2024, Tian et al., 2024, Yu et al., 2023a,b] apply AR modeling to images via next-token prediction, mimicking AR in language models [Vaswani, 2017]. This approach requires two key steps: (1) tokenizing an image into discrete tokens, and (2) modeling the tokens’ unidirectional generation process.

For tokenization, a quantized autoencoder such as VQGAN [Esser et al., 2021] is often used to convert the image feature map $\mathbf{f} \in \mathbb{R}^{(h \cdot w) \times C}$ to discrete tokens $\mathbf{z} \in [V]^{(h \cdot w)}$:

$$\mathbf{f} = \mathcal{E}(\mathbf{x}), \quad \mathbf{z} = Q(\mathbf{f}), \tag{3.1}$$

where $\mathbf{x} \in \mathbb{R}^{h' \times w' \times 3}$ denotes the raw image, $\mathcal{E}(\cdot)$ is an encoder, and $Q(\cdot)$ is a quantizer. The quantizer typically includes a learnable Codebook $\in \mathbb{R}^{V \times C}$ containing V vectors with C dimensions.

The quantization process $\mathbf{z} = Q(\mathbf{f})$ maps each feature vector \mathbf{f}^i to the code index \mathbf{z}^i of its nearest code w.r.t. the Euclidean distance:

$$\mathbf{z}_j = \arg \min_{v \in [V]} \|\text{lookup}(\text{Codebook}, v) - \mathbf{f}_j\|_2, \quad (3.2)$$

where $\text{lookup}(\text{Codebook}, v)$ means taking the v -th vector in codebook, \mathbf{z}_j and \mathbf{f}_j means j -th discrete token and feature map, respectively.

Quantized autoencoder training involves reconstructing the image and minimizing a compound loss:

$$\begin{aligned} \hat{\mathbf{f}} &= \text{lookup}(\mathbf{Z}, \mathbf{z}), \quad \hat{\mathbf{x}} = \mathcal{D}(\hat{\mathbf{f}}), \\ \mathcal{L} &= \|\mathbf{x} - \hat{\mathbf{x}}\|_2 + \|\mathbf{f} - \hat{\mathbf{f}}\|_2 + \lambda_P \mathcal{L}_P(\hat{\mathbf{x}}) + \lambda_G \mathcal{L}_G(\hat{\mathbf{x}}), \end{aligned} \quad (3.3)$$

where $\mathcal{D}(\cdot)$ is the decoder, $\mathcal{L}_P(\cdot)$ is a perceptual loss, and $\mathcal{L}_G(\cdot)$ is a discriminative loss. Using this tokenizer, a continuous image \mathbf{x} can be discretized into a sequence of categorical tokens $\mathbf{z} = (z_1, \dots, z_I)$. Conversely, generated tokens can be detokenized and then decoded back into a continuous image (i.e., realizing image generation).

Autoregressive Token Generation model predicts tokens sequentially, by factorizing the likelihood of a sequence $\mathbf{z} = (z_1, \dots, z_I)$ as:

$$p(z_1, z_2, \dots, z_I) = \prod_{t=1}^T p(z_t | z_1, z_2, \dots, z_{t-1}). \quad (3.4)$$

In the traditional AR image generation models [Esser et al., 2021, Sun et al., 2024, Tian et al., 2024, Yu et al., 2023a,b] (see Fig.2), $\{z_i\}_{t=1}^T$ are discrete tokens. However, the discrete tokens $\{z_i\}_{t=1}^T$ are not directly generated by the AR model. In fact, the autoregressive model produces a continuous-valued C -dim vector $\mathbf{z}_i \in \mathbb{R}^C$, which is then projected by a V -way classifier matrix $\mathbf{W} \in \mathbb{R}^{C \times V}$ to $z_i \in [V]$. In other words, one can use Eq.3.4 and an additional projector to generate a sequence of categorical tokens, and then use Eq.3.3 to decoder back to the image space.

Continuous AR. Recent work [Li et al., 2024, Tschannen et al., 2023] formulate the probability distribution $p(\mathbf{f}_i | \mathbf{z}_i)$ to model the detokenization for continuous tokens, where $\mathbf{f}_i \in \mathbb{R}^C$ is the t -th image patch’s feature map and $\mathbf{z}_i \in \mathbb{R}^D$ is the corresponding AR model’s output *continuous token*. MAR [Li et al., 2024] uses diffusion models to define the loss function and sampler, as shown in Fig.2 (c). MAR and its follow-up work [Fan et al., 2024] achieve state-of-the-art performance in image generation, showing the promising potential of continuous AR in the visual generation.

Efficiency Bottlenecks of Continuous AR Models. Continuous AR models face two main efficiency challenges: ❶ Token-by-token generation: Similar to LLMs, the sequential nature of generation limits efficiency [Yuan et al., 2024]. In these models, each token is produced based on all the previously generated tokens, which means that the process cannot be easily parallelized. This sequential dependency results in longer computation times, especially for generating lengthy tokens (corresponding to high-resolution images or videos). ❷ Diffusion sampling: [Song et al., 2020a] diffusion models require a large number of iterative denoising steps to generate a single sample, each of which must be executed sequentially [Song et al., 2020a].

We propose a hierarchical framework for addressing these issues, in which continuous token generation and continuous detokenization are realized in a hierarchical manner. By doing so, we are able to improve the efficiency of the continuous AR model as well as maintain its effectiveness.

3.2 Multistage Autoregressive Token Generation

Targeting the ❶ efficiency challenge, we introduce a stage-by-stage continuous tokens AR generation model to enhance the efficiency of token generation. Our method reimagines autoregressive image modeling by transitioning from a “next-token prediction” paradigm to a “next-stage prediction” strategy, as illustrated in Figs.1 and 2. In this framework, the autoregressive unit evolves from a single token to an *entire token map*. The process begins by encoding a feature map $\mathbf{M} = [z_i, \dots, z_{(h \cdot w)}] \in \mathbb{R}^{(h \cdot w) \times C}$ into a sequence of S -stage token maps $(\mathbf{M}_1, \mathbf{M}_2, \dots, \mathbf{M}_S)$. Each successive map increases in resolution from $h_1 \times w_1$ to $h_S \times w_S$, with the final map m_S matching the original feature map’s dimensions $(h \cdot w)$. The autoregressive likelihood can be formulated as:

$$p(\mathbf{M}_1, \mathbf{M}_2, \dots, \mathbf{M}_S) = \prod_{s=1}^S p(\mathbf{M}_s | \mathbf{M}_1, \mathbf{M}_2, \dots, \mathbf{M}_{s-1}). \quad (3.5)$$

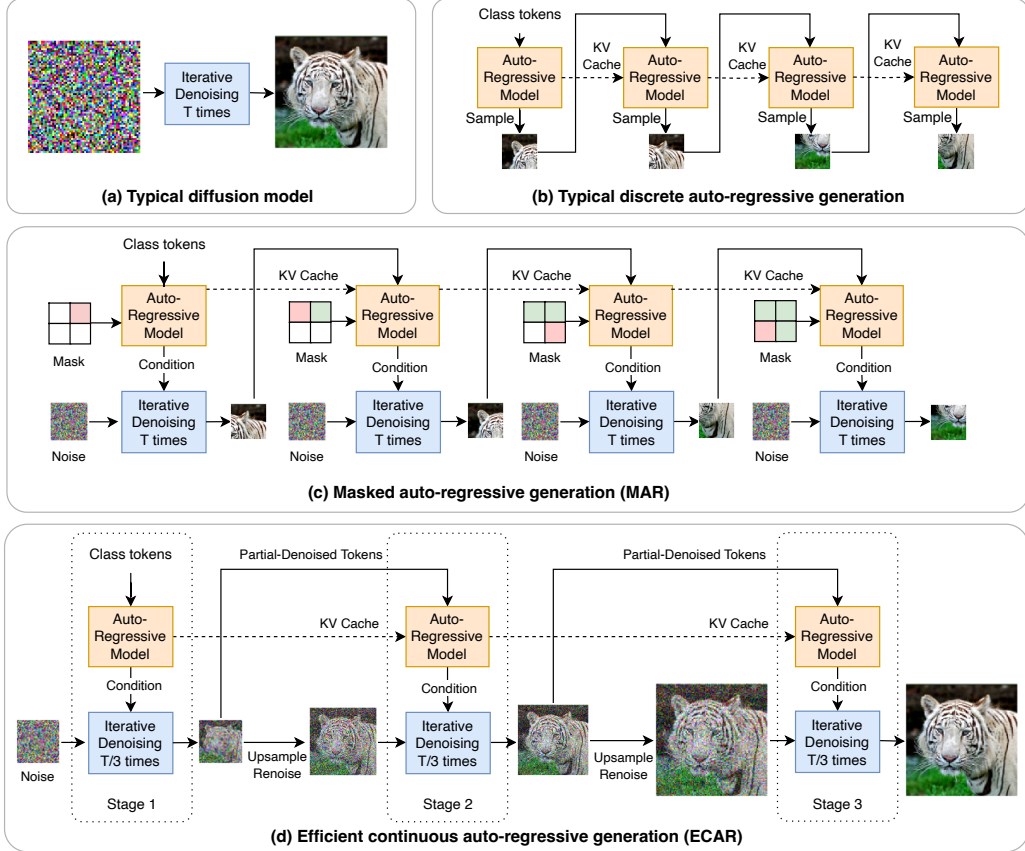


Figure 2: **(a)** Diffusion/Flow-matching model: Generates images through multiple iterations of denoising/velocity network inference. **(b)** Traditional AR Transformer: Sequentially generates discrete tokens, followed by codebook-based detokenization. **(c)** Continuous Masked AR [Li et al., 2024]: Sequentially produces continuous tokens, which are transformed into image patches via a diffusion model. **(d)** E-CAR: Introduces two key innovations: multi-stage continuous token generation and **(Sec.3.3) multi-stage flow** for efficient continuous token generation and token-to-image detokenization, respectively. Using the upsample and renoise technique [Jin et al., 2024], we can correspondingly reduce the number of steps for flow matching at each stage, enhancing the efficiency of the continuous token detokenization process.

Here, each autoregressive unit $\mathbf{M}_s \in \mathbb{R}^{(h_s \cdot w_s) \times C}$ represents the token map at stage s , encompassing $h_s \cdot w_s$ continuous tokens. The preceding sequence $(\mathbf{M}_1, \mathbf{M}_2, \dots, \mathbf{M}_{s-1})$ functions as a “prefix” [Yuan et al., 2024] for m_s . During the s -th autoregressive step, our model generates distributions for all $h_s \cdot w_s$ tokens in m_s concurrently. This parallel generation is conditioned on both the prefix and the stage-specific positional embedding map. We term this “next-stage prediction” approach Multi-stage Continuous Autoregressive, as depicted in Fig. 2.

Efficiency Benefit. The designed multi-stage continuous token generation offers significant computational advantages over the vanilla continuous AR. Theoretically, our method achieves a time complexity of $\mathcal{O}(n^2)$, where n is the number of tokens representing an image. In contrast, the vanilla continuous AR method has a time complexity of $\mathcal{O}(n^3)$. This improvement results in our approach being n times faster than the vanilla method. More details can be found in the Supplementary Materials. We would like to highlight that this efficiency gain becomes increasingly significant as we move towards long-sequence token generation (e.g., higher-resolution images or video generation).

3.3 Multistage Flow Matching for Fast Sampling from Continuous Token

After we get the set of continuous tokens $\{\mathbf{M}_s\}_{s=1}^S$, we hope to get a sampler that can draw samples from the distribution $\mathbf{F}_S \sim p(\mathbf{F}_S | \mathbf{M}_S)$ at inference time, i.e., generate image patches’ embeddings

based on the output tokens. Targeting the $\textcircled{2}$ efficiency challenge, we model this sampler under the framework using multistage flow [Liu et al., 2022, Lipman et al., 2022, Liu et al., 2024b, Xie et al., 2024] to improve the continuous detokenization efficiency.

Problem Formulation. Consider the continuous-valued token map at S -th stage $\mathbf{M}_S \in \mathbb{R}^{(h_s \cdot w_s) \times D}$, and the ground-truth image patch embeddings $\mathbf{F}^{(S)} \in \mathbb{R}^{(h_s \cdot w_s) \times C}$ to be predicted at this stage. Our goal is to model a probability distribution of \mathbf{F}_S conditioned on \mathbf{M}_S , that is, $p(\mathbf{F}^{(S)} | \mathbf{M}_S)$. In the context of optimal transport, we hope to find a velocity model, optimal transport from $\mathbf{n} | \mathbf{M}_S \sim \pi_0$ to $\mathbf{F}^{(S)} | \mathbf{M}_S \sim \pi_1$. For simple sampling, π_0 commonly be set as a normal distribution.

Flow Matching [Liu, 2022, Liu et al., 2022, Ma et al., 2024, Jin et al., 2024] is a unified ODE-based framework for generative modeling and domain transfer. It provides an approach for learning a transport mapping T between two distributions π_0 and π_1 . Specifically, flow Matching learns to transfer π_0 to π_1 via an ordinary differential equation (ODE), or flow model

$$\frac{d\mathbf{F}_t^{(S)}}{dt} = v_\theta(\mathbf{F}^{(S)}, t | \text{cond} = \mathbf{M}_S), \quad \text{initialized from } \mathbf{F}_0^{(S)} \sim \pi_0 = \mathcal{N}(\mathbf{0}, \mathbf{I}), \text{ s.t. } \mathbf{F}_1^{(S)} \sim \pi_1, \quad (3.6)$$

where cond is the condition variable, it can be a class or a text embedding, and $v_\theta : \mathbb{R}^d \times [0, 1] \times \mathbb{R}^D \rightarrow \mathbb{R}^d$ is a velocity field, learned by minimizing a mean square objective:

$$\min_{v_\theta} \mathbb{E}_{((F_S)_0, (F_S)_1) \sim \gamma, z \sim \mathcal{D}_{\text{cond}}} \left[\int_0^1 \left\| \frac{d}{dt} \mathbf{F}_t^{(S)} - v_\theta(\mathbf{F}_t^{(S)}, t | \mathbf{M}_S) \right\|^2 dt \right], \quad (3.7)$$

with $\mathbf{F}_t^{(S)} = \phi(\mathbf{F}_0^{(S)}, \mathbf{F}_1^{(S)}, t)$ where $\mathcal{D}_{\text{cond}}$ is the collection of conditions, $\mathbf{F}_t^{(S)} = \phi(\mathbf{F}_0^{(S)}, \mathbf{F}_1^{(S)}, t)$ is any time-differentiable interpolation between $\mathbf{F}_0^{(S)}$ and $\mathbf{F}_1^{(S)}$, with $\frac{d}{dt} \mathbf{F}_t^{(S)} = \partial_t \phi(\mathbf{F}_0^{(S)}, \mathbf{F}_1^{(S)}, t)$. The γ is any coupling of (π_0, π_1) . A simple example of γ is the independent coupling $\gamma = \pi_0 \times \pi_1$, which can be sampled empirically from unpaired observed data from π_0 and π_1 . Usually, v_θ is parameterized as a deep neural network and Eq.3.7 is solved approximately with stochastic gradient methods. Different specific choices of the interpolation process $\mathbf{F}_1^{(S)}$ result in different algorithms. As shown in [Liu, 2022], the commonly used denoising diffusion implicit model (DDIM) [Song et al., 2020a] and the probability flow ODEs of [Song et al., 2020b] correspond to $\mathbf{F}_t^{(S)} = \alpha_t \mathbf{F}_0^{(S)} + \beta_t \mathbf{F}_1^{(S)}$, with specific choices of time-differentiable sequences α_t, β_t (see [Liu, 2022, Liu et al., 2024b] for details). In rectified flow [Liu, 2022], the authors suggested a simpler choice of

$$\mathbf{F}_t^{(S)} = (1-t)\mathbf{F}_0^{(S)} + t\mathbf{F}_1^{(S)} \implies \frac{d}{dt} \mathbf{F}_t^{(S)} = \mathbf{F}_1^{(S)} - \mathbf{F}_0^{(S)}. \quad (3.8)$$

Simple Flow Sampler. Once we obtain a well-trained velocity model v_θ through optimization of Eq. 3.7, we can sample image patches’s embedding \mathbf{F}_S conditioned on the continuous token map \mathbf{M}_S . The sampling process involves approximating the ODE in Eq. 3.6 using numerical methods. The most common approach for this approximation is the forward Euler method, which discretizes the continuous ODE into finite steps:

$$\mathbf{F}_{t+\Delta t}^{(S)} = \mathbf{F}_t^{(S)} + \Delta t \cdot v_\theta(\mathbf{F}_t^{(S)}, t | \text{cond} = \mathbf{M}_S), \quad (3.9)$$

where $t \in \{0, \frac{1}{N}, \frac{2}{N}, \dots, \frac{N-1}{N}\}$ and $\Delta t = \frac{1}{N}$ is the step size, N is the total number of simulation steps, $\mathbf{F}_t^{(S)}$ represents the state at time t , and $v(\mathbf{F}_t^{(S)}, t)$ is the velocity predicted by our trained model. The sampling process starts at $t = 0$ and iteratively applies this update equation N times until reaching $t = 1$, thereby transforming the initial noise distribution into the desired sample distribution.

However, directly using full-size token map \mathbf{M}_S to generate full-size feature map $\mathbf{F}^{(S)}$ in the final stage is not optimal for efficiency, specifically in our stage-wise token generation case. We hope to fully leverage the low-resolution token maps. Therefore, to leverage our multi-stage token generation framework and accelerate sampling, we propose a multi-stage sampling strategy that aligns with the hierarchical nature of our token generation process.

Multi-stage Flow. To reduce redundant computation in early steps, we propose a multistage flow approach that operates at multiple resolutions. We interpolate the flow between the feature map and compressed low-resolution noise, progressively increasing the resolution at each stage, as shown in Fig.2.d.

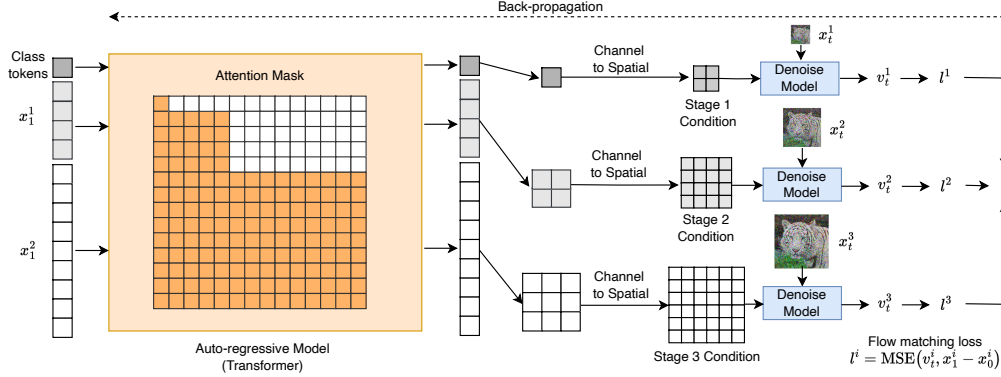


Figure 3: **Training of E-CAR.** Our model combines multistage autoregressive token generation with progressive flow matching. The AR transformer (left) generates continuous token maps using a multistage causal attention mask, which are then transformed to spatial conditions for each stage. Each stage’s token map conditions its corresponding flow model, enabling progressive reconstruction of image latents at different resolutions. The flow matching loss is computed between the predicted velocity and the ground truth trajectory at each stage, with back-propagation through the entire pipeline for end-to-end training.

Suppose we have S stages, each corresponding to a resolution level, with each stage halving the spatial dimensions of the previous one. We partition the time interval $[0, 1]$ into S segments: Stage s corresponds to the time interval $t \in [t_{s-1}, t_s]$, where $t_s = \frac{s}{S}$ for $s = 1, 2, \dots, S$. At each stage s , we define the rescaled time within the stage: $\tau = \frac{t-t_{s-1}}{t_s-t_{s-1}} \in [0, 1]$. The target feature map at the current resolution:

$$\mathbf{F}_1^{(s)} = \text{Down}(\mathbf{F}_1, 2^{S-s}), \quad (3.10)$$

where \mathbf{F}_1 is the ground-truth feature map $\mathbf{F}^{(S)}$, $\text{Down}(\cdot, k)$ denote downsampling by a factor of k .

The initial noise feature map at the current resolution $\mathbf{F}_0^{(s)}$:

$$\mathbf{F}_0^{(s)} = \begin{cases} \text{Down}(\mathbf{F}_0, 2^{S-1}), & \text{if } s = 1, \\ \text{Up}(\mathbf{F}_0^{(s-1)}), & \text{if } s > 1, \end{cases} \quad (3.11)$$

where \mathbf{F}_0 is the initial noise sample (e.g., Gaussian noise), and $\text{Up}(\cdot)$ denotes upsampling by a factor of 2. Within stage s , we interpolate between $\mathbf{F}_0^{(s)}$ and $\mathbf{F}_1^{(s)}$ using the rescaled time τ :

$$\hat{\mathbf{F}}_t^{(s)} = (1 - \tau)\mathbf{F}_0^{(s)} + \tau\mathbf{F}_1^{(s)}. \quad (3.12)$$

This interpolation ensures that feature maps at each stage have matching dimensions, allowing us to perform computations efficiently at each resolution level. Only the final stage ($s = S$) operates at full resolution, where no downsampling is applied: $\mathbf{F}_1^{(S)} = \mathbf{F}_1$. More details about the multistage flow can be found in [Jin et al., 2024] and our Appendix.

Efficiency Benefits. By performing computations at progressively higher resolutions, we can reduce the computational burden. Early stages operate on downsampled feature maps, which are much smaller in size, thus requiring fewer computations. Only the final stage processes the full-resolution feature map. This multistage approach effectively reduces the overall computational cost by a factor of approximately $1/S$, assuming uniform time partitioning and resolution scaling.

Latent Space Technique. Even though the whole story is on how to model between continuous token map \mathbf{M}_s and image feature map $\mathbf{F}^{(s)}$, the latent space technique for high-resolution image synthesis [Rombach et al., 2022] can also be easily removed out of our pipeline (*i.e.*, directly used in the image domain $\mathbf{X}^{(s)}$ without latent space).

3.4 Training Loss

The training of E-CAR involves optimizing both the multistage autoregressive token generation model and the multistage flow matching model. At each stage, our goal is to reconstruct the image’s

latent representations at varying resolutions, ensuring that the model learns to generate accurate representations progressively. Specifically, for each stage s : **Continuous Token Generation:** We generate the continuous token map \mathbf{M}_s using the multistage autoregressive (AR) model, as described in Sec. 3.2. This token map serves as the conditioning information for the flow model at stage s . **Image Latent Reconstruction:** We reconstruct the image’s latent representation \mathbf{F}_s at resolution level s using the multistage flow model. The reconstruction is conditioned on the continuous token map \mathbf{M}_s . Specifically, we sample $\hat{\mathbf{F}}^{(s)}$ by solving the ODE defined in Eq. (3.9) using the velocity model v_θ :

$$\hat{\mathbf{F}}^{(s)} = \text{ODE}[v_\theta](\mathbf{F}_0^{(s)} \mid \mathbf{M}_s), \quad (3.13)$$

where $\mathbf{F}_0^{(s)}$ is the initial noise sample at stage s , typically a downsampled noisy image. **Flow Matching Loss Computation:** We compute the flow matching loss l_{flow}^s at stage s using the time-dependent interpolated latent representations $\hat{\mathbf{F}}_t$ and their derivatives:

$$l_{\text{flow}}^s = \mathbb{E}_{(\mathbf{F}_0^{(s)}, \mathbf{F}_1^{(s)}), t \in [t_{s-1}, t_s]} \left[\left\| \frac{d\hat{\mathbf{F}}_t^{(s)}}{dt} - v_\theta(\hat{\mathbf{F}}_t^{(s)}, t \mid \mathbf{M}_s) \right\|^2 \right], \quad (3.14)$$

where $\mathbf{F}_1^{(s)}$ is the ground-truth image latent at stage s , and $\frac{d\hat{\mathbf{F}}_t^{(s)}}{dt} = \mathbf{F}_1^{(s)} - \mathbf{F}_0^{(s)}$ due to linear interpolation (see Fig.3).

This multi-stage loss encourages the model to generate accurate representations at various resolutions, ultimately leading to high-quality final outputs. To dynamically balance the contributions of different stages to the overall loss, we employ the GradNorm technique [Chen et al., 2018b]. This adaptive weighting method automatically adjusts the stage-specific weights w_s during training.

4 Experiments

We detail the experimental setup and model configurations in Sec. 4.1, followed by an analysis of the quantitative and qualitative performance of our approach in Sec. 4.2 and Sec. 4.4. Finally, we demonstrate the effectiveness of each component in our model in Sec.4.5.

4.1 Experimental Setup

We train the image generation models on ImageNet [Deng et al., 2009] train dataset at 256×256 resolution. The image tokenizer is from SDXL [Podell et al.], which is a VAE that transform the image to the latent space with 8x reduction. The latent resolution is 32×32 when the image resolution is 256×256 . All models are trained with the settings: AdamW optimizer with learning rate of $1e-4$, no weight decay, and the batch size of 256. We use 8 NVIDIA A100 GPUs to train each model and the TF32 dataformat to accelerate the training process.

Table 1: Model configurations.

		E-CAR-S	E-CAR-B	E-CAR-L
AR	Layers	10	20	24
	Hidden size	768	1024	1152
	Heads	6	16	16

Model. To demonstrate the scalability of E-CAR, we trained different size of models, E-CAR- $\{S, B, L\}$. The model configurations are shown in Table 1. The auto-regressive model (AR) takes ViT backbone [Dosovitskiy, 2020]. There are three auto-regressive stages to generate image at latent space, and the latent resolutions of these stages are $\{8, 16, 32\}$. For each stage, we use a diffusion model with much smaller number of Transformer layers than the auto-regressive model. Therefore, the diffusion model is efficient to iteratively denoise on the latent space. We use the adaptive layer normalization (adaLN) [Peebles & Xie, 2023] to incorporate the conditional information into the diffusion process. Unlike DiT [Peebles & Xie, 2023] takes the class condition as a global information, the condition from AR model is spatially variant in E-CAR. That is, the condition is different at each spatial location in diffusion model.

Table 2: Quantitative results: 256×256 image generation with classifier-free guidance (CFG). IS is inception score, P is precision and R is recall.

Model	Params	FLOPs	FID↓	IS↑	P↑	R↑
DiT-XL/2 (7M)	675M	60T	2.27	278	0.83	0.57
MAR-B	208M	18T	2.31	282	0.82	0.57
MAR-L	479M	34T	1.78	296	0.81	0.60
MAR-H	943M	60T	1.55	304	0.81	0.62
E-CAR-S (400K)	155M	1T	9.21	303	0.85	0.29
E-CAR-B (400K)	511M	3.2T	7.02	309	0.84	0.38
E-CAR-L (800K)	854M	5.8T	4.99	274	0.85	0.41

Table 3: 256×256 image generation latency (s) without CFG.

Model	Params	4090	i9-13900K	Apple M2
Batchsize=1				
DiT-B/2	130M	1.44	17.94	8.60
DiT-L/2	458M	2.73	59.70	16.50
DiT-XL/2	675M	3.42	75.35	18.90
MAR-B	208M	40.61	146.26	-
MAR-L	479M	45.37	257.02	-
MAR-H	943M	59.54	463.62	-
E-CAR-S	155M	0.38	3.92	2.03
E-CAR-B	511M	0.68	10.95	3.35
E-CAR-L	854M	0.94	18.22	4.62

Metric. We use the same evaluation metrics as Guided Diffusion, FID [Heusel et al., 2017], Inception Score (IS) [Salimans et al., 2016], Improved Precision and Recall [Kynkäänniemi et al., 2019]. In general, Frechet Inception Distance (FID) and Inception Score can measure the quality of the generated images, and recall score can measure the diversity of generated images. We generate 50K images with 250 total denoising steps. Each stage takes 1/3 of the total denoising steps.

4.2 Quantitative Results

To quantitatively evaluate the performance of E-CAR image generation, we trained the E-CAR S,B,L models for 400K iterations. We choose two widely used model series to compare, including DiT [Peebles & Xie, 2023] and MAR [Li et al., 2024].

The results are shown in Table 2. The E-CAR-L model achieves a computational performance of 5.8 TFLOPs for generating 256×256 images with classifier-free guidance (CFG), which is a mere 9.7% of the capabilities seen in both the MAR-H and DiT-XL/2 models. E-CAR-L achieve highest inception score and precision among three types of model. Though E-CAR-L has a higher FID compared with MAR-H and DiT-XL/2, it’s important to highlight that due to time constraints, our E-CAR models have only undergone 400K training iterations, significantly fewer than the 7 million iterations typical for DiT and MAR models. As shown in fig 6, at 400K iterations, the model loss is continuously decreasing, suggesting that further training could potentially result in a lower FID. Our findings demonstrate that E-CAR-L significantly diminishes computational expenses while maintaining a high standard of image generation quality.

4.3 Inference Efficiency Analysis

To evaluate the inference efficiency of E-CAR, we deploy the model on different devices including NVIDIA 4090 24G GPU, Intel i9-13900K CPU with 32G memory, and Apple M2 16G on Macbook Air. The batchsize of inference is set to 1. The result is shown in Table 3. The generation time of E-CAR-L model on 4090 GPU is less than 1 second. In comparison to MAR models, E-CAR models achieve a substantial speedup from $63 \times$ to $107 \times$ on NVIDIA 4090 GPUs, and $25 \times$ to $37 \times$ on Intel



Figure 4: Samples from different models with the same noise.

i9-13900K CPUs. MAR results for the Apple M2 are not listed, as the platform is not supported and encountered errors during testing. When compared with DiT models, despite having a slightly higher number of model parameters than DiT models, our models still deliver considerable acceleration on all test devices. E-CAR models achieve $3.6\times - 4.0\times$ speedup on 4090 GPUs, $4.1\times - 5.5\times$ speedup on i9-13900K CPU, and $4.1\times - 4.9\times$ speedup on Apple M2 chips.

Efficiency of E-CAR. Here, we provide a straightforward explanation of why E-CAR is both more efficient and effective than traditional AR image generation models. The efficiency of E-CAR stems from three key factors: (1) Hierarchical Continuous Token Generation: As described in Sec. 3.2, our stage-wise approach reduces the computational complexity from $\mathcal{O}(n^3)$ to $\mathcal{O}(n^2)$, where n is the number of tokens. (2) Efficient Detokenization: The multistage flow in Sec.3.3 offers a more efficient alternative to diffusion-based approaches for transforming tokens into images. Diffusion-based detokenizer needs (3) Parallel Processing: Unlike token-by-token generation, E-CAR can generate the entire stack of tokens for an image simultaneously. This enables parallel processing during token recovery, further enhancing efficiency.

Effectiveness in Image Generation. The effectiveness of E-CAR in image generation is rooted in two principles: (1) Continuous Representation: Images are inherently continuous signals. By operating in a continuous token space, E-CAR aligns more closely with the natural structure of images, a widely accepted inductive bias in computer vision. It echoes the finding in [Yu et al., 2024] that representation space is important for generative models’ training. (2) Hierarchical Architecture: The stage-wise generation process of E-CAR mirrors the hierarchical nature of visual information, from coarse structures to fine details. This approach allows the model to generate images at multiple scales effectively.

4.4 Qualitative Results

We show the generated images of E-CAR models with three different model size in Figure 4. We can observe that our method is able to generate high quality images with 400K training rounds. Among three models, images generated by E-CAR-L has highest visual fidelity, demonstrating our method has scaling behavior.

4.5 Ablation Study

To show the effective of the E-CAR architecture, we replace the layers in auto-regressive model with layers in denoising model, that is, only the low resolution image is sent to the next stage.

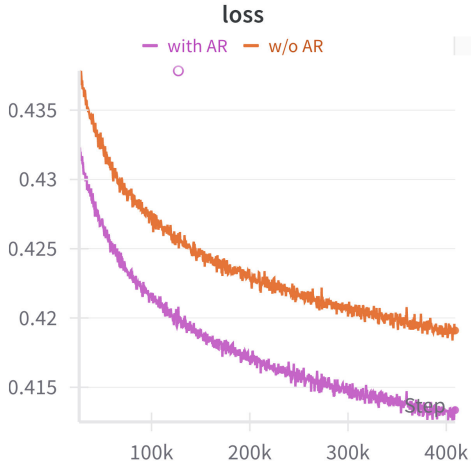


Figure 5: Ablation study of AR.

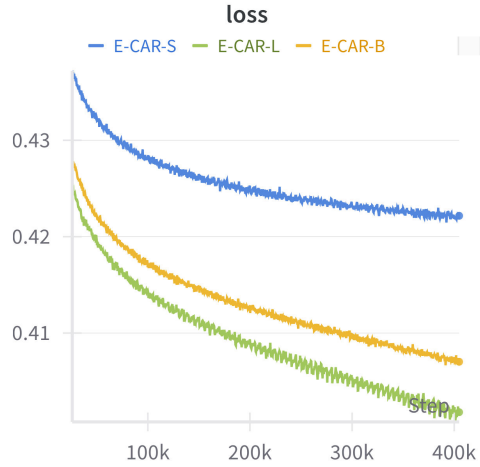


Figure 6: Training loss.

The results are shown in Figure 5. It shows that by using the auto-regressive model, the loss can decrease significantly quickly. This indicate that the auto-regressive can plan the generation process in high-level, and the denoising model is only focused on low-level denoising process.

5 Conclusion

We introduce E-CAR, a method enhancing continuous AR image generation efficiency with two innovations: 1) stage-wise progressive token map generation that reduces computation by generating tokens at increasing resolutions in parallel, and 2) multistage flow-based distribution modeling that transforms only partial-denoised distributions at each stage comparing to complete denoising in normal diffusion models. Experiments show that E-CAR achieves comparable image quality to prior work while requiring $10\times$ fewer FLOPs and providing a $5\times$ speedup for 256×256 image generation.

Acknowledgment: We would like to express our gratitude to Xuefei Ning for her invaluable guidance and support throughout this research endeavor. We are also grateful to the NICS-efc Lab and Infinigence AI for their substantial support.

References

- Josh Achiam, Steven Adler, Sandhini Agarwal, Lama Ahmad, Ilge Akkaya, Florencia Leoni Aleman, Diogo Almeida, Janko Altschmidt, Sam Altman, Shyamal Anadkat, et al. Gpt-4 technical report. *arXiv preprint arXiv:2303.08774*, 2023.
- Mark Chen, Alec Radford, Rewon Child, Jeffrey Wu, Heewoo Jun, David Luan, and Ilya Sutskever. Generative pretraining from pixels. In *ICML*, 2020.
- Xi Chen, Nikhil Mishra, Mostafa Rohaninejad, and Pieter Abbeel. Pixelsnail: An improved autoregressive generative model. In *ICML*, 2018a.
- Zhao Chen, Vijay Badrinarayanan, Chen-Yu Lee, and Andrew Rabinovich. Gradnorm: Gradient normalization for adaptive loss balancing in deep multitask networks. In *ICML*, 2018b.
- Florinel-Alin Croitoru, Vlad Hondru, Radu Tudor Ionescu, and Mubarak Shah. Diffusion models in vision: A survey. *TPAMI*, 2023.
- Jia Deng, Wei Dong, Richard Socher, Li-Jia Li, Kai Li, and Li Fei-Fei. Imagenet: A large-scale hierarchical image database. In *CVPR*, 2009.
- Alexey Dosovitskiy. An image is worth 16x16 words: Transformers for image recognition at scale. *arXiv preprint arXiv:2010.11929*, 2020.
- Patrick Esser, Robin Rombach, and Bjorn Ommer. Taming transformers for high-resolution image synthesis. In *CVPR*, 2021.
- Patrick Esser, Sumith Kulal, Andreas Blattmann, Rahim Entezari, Jonas Müller, Harry Saini, Yam Levi, Dominik Lorenz, Axel Sauer, Frederic Boesel, et al. Scaling rectified flow transformers for high-resolution image synthesis. In *ICML*, 2024.
- Lijie Fan, Tianhong Li, Siyang Qin, Yuanzhen Li, Chen Sun, Michael Rubinstein, Deqing Sun, Kaiming He, and Yonglong Tian. Fluid: Scaling autoregressive text-to-image generative models with continuous tokens. *arXiv preprint arXiv:2410.13863*, 2024.
- Karol Gregor, Ivo Danihelka, Andriy Mnih, Charles Blundell, and Daan Wierstra. Deep autoregressive networks. In *ICML*, 2014.
- Martin Heusel, Hubert Ramsauer, Thomas Unterthiner, Bernhard Nessler, and Sepp Hochreiter. Gans trained by a two time-scale update rule converge to a local nash equilibrium. *NeurIPS*, 2017.
- Jonathan Ho, Ajay Jain, and Pieter Abbeel. Denoising diffusion probabilistic models. *NeurIPS*, 2020.
- Jordan Hoffmann, Sebastian Borgeaud, Arthur Mensch, Elena Buchatskaya, Trevor Cai, Eliza Rutherford, Diego de Las Casas, Lisa Anne Hendricks, Johannes Welbl, Aidan Clark, et al. Training compute-optimal large language models. *arXiv preprint arXiv:2203.15556*, 2022.
- Albert Q Jiang, Alexandre Sablayrolles, Arthur Mensch, Chris Bamford, Devendra Singh Chaplot, Diego de las Casas, Florian Bressand, Gianna Lengyel, Guillaume Lample, Lucile Saulnier, et al. Mistral 7b. *arXiv preprint arXiv:2310.06825*, 2023.
- Yang Jin, Zhicheng Sun, Ningyuan Li, Kun Xu, Hao Jiang, Nan Zhuang, Quzhe Huang, Yang Song, Yadong Mu, and Zhouchen Lin. Pyramidal flow matching for efficient video generative modeling. *arXiv preprint arXiv:2410.05954*, 2024.
- Jared Kaplan, Sam McCandlish, Tom Henighan, Tom B Brown, Benjamin Chess, Rewon Child, Scott Gray, Alec Radford, Jeffrey Wu, and Dario Amodei. Scaling laws for neural language models. *arXiv preprint arXiv:2001.08361*, 2020.
- Tuomas Kynkäänniemi, Tero Karras, Samuli Laine, Jaakko Lehtinen, and Timo Aila. Improved precision and recall metric for assessing generative models. In *NeurIPS*, 2019.
- Doyup Lee, Chihyeon Kim, Saehoon Kim, Minsu Cho, and Wook-Shin Han. Autoregressive image generation using residual quantization. In *Proceedings of the IEEE/CVF Conference on Computer Vision and Pattern Recognition*, pp. 11523–11532, 2022.
- Tianhong Li, Yonglong Tian, He Li, Mingyang Deng, and Kaiming He. Autoregressive image generation without vector quantization. *arXiv preprint arXiv:2406.11838*, 2024.

- Yaron Lipman, Ricky TQ Chen, Heli Ben-Hamu, Maximilian Nickel, and Matt Le. Flow matching for generative modeling. *arXiv preprint arXiv:2210.02747*, 2022.
- Dongyang Liu, Shitian Zhao, Le Zhuo, Weifeng Lin, Yu Qiao, Hongsheng Li, and Peng Gao. Lumina-mgpt: Illuminate flexible photorealistic text-to-image generation with multimodal generative pretraining. *arXiv preprint arXiv:2408.02657*, 2024a.
- Qiang Liu. Rectified flow: A marginal preserving approach to optimal transport. *arXiv preprint arXiv:2209.14577*, 2022.
- Xingchao Liu, Chengyue Gong, and Qiang Liu. Flow straight and fast: Learning to generate and transfer data with rectified flow. *arXiv preprint arXiv:2209.03003*, 2022.
- Xingchao Liu, Xiwen Zhang, Jianzhu Ma, Jian Peng, et al. InstafLOW: One step is enough for high-quality diffusion-based text-to-image generation. In *ICLR*, 2024b.
- Nanye Ma, Mark Goldstein, Michael S Albergo, Nicholas M Boffi, Eric Vanden-Eijnden, and Saining Xie. Sit: Exploring flow and diffusion-based generative models with scalable interpolant transformers. *arXiv preprint arXiv:2401.08740*, 2024.
- William Peebles and Saining Xie. Scalable diffusion models with transformers. In *Proceedings of the IEEE/CVF International Conference on Computer Vision*, pp. 4195–4205, 2023.
- Pablo Pernias, Dominic Rampas, Mats L Richter, Christopher J Pal, and Marc Aubreville. Würstchen: An efficient architecture for large-scale text-to-image diffusion models. *arXiv preprint arXiv:2306.00637*, 2023.
- Dustin Podell, Zion English, Kyle Lacey, Andreas Blattmann, Tim Dockhorn, Jonas Müller, Joe Penna, and Robin Rombach. Sdxl: Improving latent diffusion models for high-resolution image synthesis. In *The Twelfth International Conference on Learning Representations*.
- Alec Radford. Improving language understanding by generative pre-training. 2018.
- Ali Razavi, Aaron Van den Oord, and Oriol Vinyals. Generating diverse high-fidelity images with vq-vae-2. *Advances in neural information processing systems*, 32, 2019.
- Robin Rombach, Andreas Blattmann, Dominik Lorenz, Patrick Esser, and Björn Ommer. High-resolution image synthesis with latent diffusion models. In *CVPR*, 2022.
- Chitwan Saharia, William Chan, Saurabh Saxena, Lala Li, Jay Whang, Emily L Denton, Kamyar Ghasemipour, Raphael Gontijo Lopes, Burcu Karagol Ayan, Tim Salimans, et al. Photorealistic text-to-image diffusion models with deep language understanding. *NeurIPS*, 2022.
- Tim Salimans, Ian Goodfellow, Wojciech Zaremba, Vicki Cheung, Alec Radford, and Xi Chen. Improved techniques for training gans. *Advances in neural information processing systems*, 29, 2016.
- Jascha Sohl-Dickstein, Eric Weiss, Niru Maheswaranathan, and Surya Ganguli. Deep unsupervised learning using nonequilibrium thermodynamics. In *ICML*, 2015.
- Jiaming Song, Chenlin Meng, and Stefano Ermon. Denoising diffusion implicit models. *arXiv preprint arXiv:2010.02502*, 2020a.
- Yang Song, Jascha Sohl-Dickstein, Diederik P Kingma, Abhishek Kumar, Stefano Ermon, and Ben Poole. Score-based generative modeling through stochastic differential equations. *ICLR*, 2020b.
- Peize Sun, Yi Jiang, Shoufa Chen, Shilong Zhang, Bingyue Peng, Ping Luo, and Zehuan Yuan. Autoregressive model beats diffusion: Llama for scalable image generation. *arXiv preprint arXiv:2406.06525*, 2024.
- Chameleon Team. Chameleon: Mixed-modal early-fusion foundation models. *arXiv preprint arXiv:2405.09818*, 2024.
- Keyu Tian, Yi Jiang, Zehuan Yuan, Bingyue Peng, and Liwei Wang. Visual autoregressive modeling: Scalable image generation via next-scale prediction. *arXiv preprint arXiv:2404.02905*, 2024.
- Hugo Touvron, Thibaut Lavril, Gautier Izacard, Xavier Martinet, Marie-Anne Lachaux, Timothée Lacroix, Baptiste Rozière, Naman Goyal, Eric Hambro, Faisal Azhar, et al. Llama: Open and efficient foundation language models. *arXiv preprint arXiv:2302.13971*, 2023a.
- Hugo Touvron, Louis Martin, Kevin Stone, Peter Albert, Amjad Almahairi, Yasmine Babaei, Nikolay Bashlykov, Soumya Batra, Prajjwal Bhargava, Shrubti Bhosale, et al. Llama 2: Open foundation and fine-tuned chat models. *arXiv preprint arXiv:2307.09288*, 2023b.

- Michael Tschannen, Cian Eastwood, and Fabian Mentzer. Givt: Generative infinite-vocabulary transformers. *arXiv preprint arXiv:2312.02116*, 2023.
- Aäron Van Den Oord, Nal Kalchbrenner, and Koray Kavukcuoglu. Pixel recurrent neural networks. In *ICML*, 2016.
- A Vaswani. Attention is all you need. *NeurIPS*, 2017.
- Shenghao Xie, Wenqiang Zu, Mingyang Zhao, Duo Su, Shilong Liu, Ruohua Shi, Guoqi Li, Shanghang Zhang, and Lei Ma. Towards unifying understanding and generation in the era of vision foundation models: A survey from the autoregression perspective. *arXiv preprint arXiv:2410.22217*, 2024.
- Lijun Yu, Yong Cheng, Kihyuk Sohn, José Lezama, Han Zhang, Huiwen Chang, Alexander G Hauptmann, Ming-Hsuan Yang, Yuan Hao, Irfan Essa, et al. Magvit: Masked generative video transformer. In *CVPR*, 2023a.
- Lijun Yu, José Lezama, Nitesh B Gundavarapu, Luca Versari, Kihyuk Sohn, David Minnen, Yong Cheng, Agrim Gupta, Xiuye Gu, Alexander G Hauptmann, et al. Language model beats diffusion–tokenizer is key to visual generation. *arXiv preprint arXiv:2310.05737*, 2023b.
- Sihyun Yu, Sangkyung Kwak, Huiwon Jang, Jongheon Jeong, Jonathan Huang, Jinwoo Shin, and Saining Xie. Representation alignment for generation: Training diffusion transformers is easier than you think. *arXiv preprint arXiv:2410.06940*, 2024.
- Zhihang Yuan, Yuzhang Shang, Yang Zhou, Zhen Dong, Chenhao Xue, Bingzhe Wu, Zhikai Li, Qingyi Gu, Yong Jae Lee, Yan Yan, et al. Llm inference unveiled: Survey and roofline model insights. *arXiv preprint arXiv:2402.16363*, 2024.
- Chunting Zhou, Lili Yu, Arun Babu, Kushal Tirumala, Michihiro Yasunaga, Leonid Shamis, Jacob Kahn, Xuezhe Ma, Luke Zettlemoyer, and Omer Levy. Transfusion: Predict the next token and diffuse images with one multi-modal model. *arXiv preprint arXiv:2408.11039*, 2024.

A Appendix

A.1 Training More Iterations

We have extended the training of E-CAR-L to 800,000 iterations, resulting in a Fréchet Inception Distance (FID) of 4.9. This represents a significant improvement compared to the 400,000 iterations, which achieved an FID of 6.5. However, we have observed that the loss has not yet converged and continues to decrease steadily. Therefore, we are continuing the training of this model for more iterations, as we believe the results will improve further.

A.2 Token Generation Efficiency Analysis

For a standard self-attention transformer, the time complexity of AR generation is $O(n^3)$, where n is the total number of image tokens.

In AR generation, tokens are generated one at a time. For the i -th token ($1 \leq i \leq n$), the model computes attention scores between the new token and all previously generated $i - 1$ tokens. The attention computation scales quadratically with the sequence length, so the time complexity for generating the i -th token is $O(i^2)$.

The total time complexity is the sum over all n tokens:

$$\begin{aligned} T_{\text{AR}} &= \sum_{i=1}^n O(i^2) \\ &= O\left(\sum_{i=1}^n i^2\right) \\ &= O\left(\frac{n(n+1)(2n+1)}{6}\right) \\ &= O(n^3). \end{aligned}$$

For a standard self-attention transformer using the multistage method with a resolution schedule, the time complexity is $O(n^2)$.

In Multistage AR generation, tokens are generated in stages with increasing resolutions. Define a sequence of stages (n_1, n_2, \dots, n_K) , where n_k is the number of tokens at stage k , and K is the total number of stages.

Assume that the number of tokens doubles at each stage (for simplicity), starting from $n_1 = 1$:

$$n_k = 2^{k-1}, \quad \text{for } 1 \leq k \leq K.$$

The cumulative number of tokens up to stage k is:

$$S_k = \sum_{i=1}^k n_i = 2^k - 1.$$

Since the total number of tokens is n , we have:

$$n = S_K = 2^K - 1 \implies K = \log_2(n + 1).$$

At each stage k , the time complexity is proportional to S_k^2 (due to the quadratic scaling of attention computation):

$$T_{\text{MultiAR}} = \sum_{k=1}^K O(S_k^2).$$

Substitute $S_k = 2^k - 1$:

$$\begin{aligned} T_{\text{MultiAR}} &= O\left(\sum_{k=1}^K (2^k - 1)^2\right) \\ &= O\left(\sum_{k=1}^K (2^{2k} - 2^{k+1} + 1)\right) \\ &= O\left(\sum_{k=1}^K 4^k - 2^{k+1} + 1\right). \end{aligned}$$

Compute each term separately and combine the sums:

$$\begin{aligned} T_{\text{MultiAR}} &= O\left(\frac{4^{K+1} - 4}{3} - 2^{K+2} + 4 + K\right) \\ &= O\left(\frac{4^{K+1}}{3} - 2^{K+2} + K + \text{constants}\right). \end{aligned}$$

Since $K = \log_2(n + 1)$, we have:

$$4^{K+1} = 2^{2(K+1)} = 2^{2(\log_2(n+1)+1)} = 4(n + 1)^2.$$

Similarly:

$$2^{K+2} = 2^{\log_2(n+1)+2} = 4(n + 1).$$

Therefore, the dominant terms in T_{MultiAR} are:

$$\begin{aligned} T_{\text{MultiAR}} &= O\left(\frac{4(n + 1)^2}{3} - 4(n + 1) + \log_2(n + 1)\right) \\ &= O(n^2). \end{aligned}$$

Comparing the time complexities:

$$\frac{T_{\text{AR}}}{T_{\text{MultiAR}}} = \frac{O(n^3)}{O(n^2)} = O(n).$$

Thus, the multistage AR method is faster than the AR method by a factor of $O(n)$ when generating an image with n tokens. The modeling and proof are inspired by VAR [Tian et al., 2024].

A.3 Upsample-Renoise in Multi-stage Flow

In the inference phase, because the interpolation of $\hat{\mathbf{F}}_t$ involves feature maps of varying dimensions across different stages, we employ an Upsampling and Re-noising module inspired by Pyramidal Flow Matching [Jin et al., 2024]. This module ensures that the Gaussian distributions are matched at each transition point by applying a linear transformation to the upsampled results. Specifically, when moving from a lower-resolution stage to a higher-resolution one, we upsample the feature map and add Gaussian noise to match the statistical properties required for flow matching. This process facilitates smooth transitions between stages and maintains consistency in the multistage flow framework.